Ionics (2022) 28:3679–3686
https://doi.org/10.1007/s11581-022-04628-x

ORIGINAL PAPER

Effect of calcination temperature on electrochemical properties of spinel-like $NiCo_2O_4$ nano-/microstructures

Manpreet Kaur[1] · Prakash Chand[2] · Hardeep Anand[1]

Received: 20 April 2022 / Revised: 20 May 2022 / Accepted: 28 May 2022 / Published online: 3 June 2022

Abstract

The current study evaluated the impact of the annealing temperature on the electrochemical characteristics of the spinel-like nickel cobaltite ($NiCo_2O_4$) nano-/microstructures. For this purpose, $NiCo_2O_4$ samples are prepared through a facile co-precipitation synthesis and calcined at two distinct temperatures of 300 °C and 500 °C. The prepared samples were characterized through X-ray diffraction (XRD), scanning electron microscope (SEM), and energy dispersive X-rays analysis (EDX). The electrochemical characterizations are carried out on prepared samples using the CHI760E electrochemical workstation to determine their suitability as active materials for supercapacitors. The results revealed the battery-type behavior of the prepared electrode materials with the highest value of specific capacity in a 500 °C calcined sample of 224 C/g at 2.00 A/g. The results of EIS are aligned with the outcomes of CV and GCD. The electrochemical analysis indicates that the 500 °C calcined temperature is appropriate for use as electrode material in supercapacitors.

Keywords Supercapacitor · Spinel · Co-precipitation · Cyclic voltammetry · Electrochemical

Introduction

The time has come when energy has become the priority of humankind. Human beings rely on energy in numerous areas, from the kitchen to the office, from house to market, and from a journey to the destination. As the need for energy expands, so does the requirement for storage devices. Due to certain limitations, traditional batteries and capacitors are unable to meet the ever-increasing demand for energy storage devices [1]. Batteries take a long time to charge in today's fast-paced environment, and capacitors are unable to provide prolonged discharge times [2]. In the last few decades, supercapacitors have achieved a lot of interest from researchers owing to their extraordinary properties of quick charging and discharging, excellent cycle stability, and larger power density [3]. In general, supercapacitors are split into three categories [4]: the first is EDLC (electric double layer capacitor), which uses carbonous materials as the working electrode material [5, 6]. The pseudocapacitor (PC) is the second type of supercapacitor that uses metal oxides or hydroxides as the electrode material and stores energy because of redox processes at the boundary of electrode and electrolyte [7]. The hybrid supercapacitors (HS) fall into the third group, with one electrode made of EDLC and the other made of PC electrode material [8, 9]. But the supercapacitor still lags the batteries in terms of energy density. The research community from all over the globe is focused on enhancing the energy density of supercapacitors. Recently, the battery-type materials have been widely produced and researched in the field of energy storage because of their richer faradaic redox reactions and higher energy density. In electrochemical studies, battery-type electrode materials have clear redox peaks and a nonlinear potential platform, but EDLC and PC materials have different patterns. As a result, the capacity of charge storage for battery-type materials is expressed in C/g rather than F/g for specific capacitance [10]. In general, the type of electrode materials, calcination temperature, synthesis method, and electrolyte deliver a significant impact on the specific capacitance of the electrode material. A high-performance SC is desirable with high specific capacitance/capacity, durable cycling

✉ Prakash Chand
prakash@nitkkr.ac.in

Manpreet Kaur
manpreet4317@gmail.com

[1] Department of Chemistry, Kurukshetra University, Kurukshetra 136119, India

[2] Department of Physics, National Institute of Technology, Kurukshetra 136119, India

stability, and low specific capacitance. Binary metal oxides have become highly attractive electrode materials in supercapacitors because of their high theoretical specific capacity [11]. Numerous spinels can be used for this purpose like Fe_3O_4, Cu_3O_4, $CuFe_2O_4$, $MnCo_2O_4$, $NiCo_2O_4$, $ZnCo_2O_4$, $MgCo_2O_4$, and $FeCo_2O_4$, and all these effectively serve outstanding electrochemical properties [4, 12, 13]. For a couple of decades, spinel $NiCo_2O_4$ has attracted considerable interest because it is not only cost-effective, plentiful, and ecologically acceptable, but it also has superior electrical conductivity and electrochemical activity to Mn- and V-based materials. There are ample factors that deliver a significant role in the electrochemical presentation of $NiCo_2O_4$ as a supercapacitor device such as the method of fabrication [14], precursor taken for synthesis, pH of the synthesis solution [15, 16], type, and concentration of electrolyte, aging period, and the temperature of calcination [17]. H. Qin et al. demonstrated a multi-responsive healable supercapacitor with magnetic Fe_3O_4@Au/polyacrylamide (MFP) as the electrode material to improve the reliability and lifespan of the device. Herein, results showed the highest areal capacitance of 1264 mF/cm^2 and restore ~ 90% of the initial value of capacitances after ten healing cycles [18]. K. Xu et al. successfully synthesized hollow $NiCo_2O_4$ nanostructures with high active surface area using freshly prepared SiO_2 nanospheres. The resulted sample yielded the highest specific capacitance of 1229 F/g at 1.0 A/g, appreciable rate performance of 83% up to 25 A/g current density, and good charging-discharging stability of 86% after 3000 cycles [19]. By producing flower-like $NiCo_2O_4$ and balancing asymmetric capacitance, Z. Wang et al. were able to overcome the shortcomings of $NiCo_2O_4$ as a supercapacitor electrode, such as a narrow operating voltage and low mass loading. As a result, even with a loading mass of up to 9 mg/cm^2, the flower-like NiCo2O4 with highly porous ultrathin petals has a high specific capacity of 350 C/g [20]. N. Zhao et al. utilized two-step electrodeposition followed by the calcination method to produce $NiCo_2O_4$@$Ni_{4.5}Co_{4.5}S_8$ on the Ni foam to obtain nanosheet morphology. The resulting sample liberated a specific discharge capacity of 369 mAh/g at 1.0 A/g and 258 mAh/g at 20 A/g and excellent cycle stability after 5000 cycles with only 4.8% loss in capacity [21]. H. Chen et al. again fabricated flowerlike $NiCo_2O_4$ nanostructures with an enhanced specific capacitance of 658 F/g at 1 A/g current density through a simple hydrothermal method [22]. The prepared NiCo2O4 sample has an extremely extended cycling lifespan, with no signs of degradation even after 10,000 cycles. Recently, A. Manalu et al. fabricated a nanocomposite of $NiCo_2O_4$ with rGO via the facile hydrothermal method and reported a specific capacitance of 289.93 F/g as pseudocapacitor [23]. No one has examined the influence of temperature of calcination on the electrochemical presentation of $NiCo_2O_4$ nanostructures to our knowledge. We synthesized $NiCo_2O_4$ at two distinct calcination temperatures, 300 °C and 500 °C, for this objective. The synthesized material was characterized by XRD for the analysis of sample purity and crystallinity. SEM analyses were performed for the morphology. To investigate the electrochemical performance, CV, GCD, and EIS were performed. From the GCD, the evaluated value of specific capacity is 224 C/g and 100C/g at current density of 2.00 A/g from NC500 and NC300, respectively. Hence, the calcination temperature influences the electrochemical performance of the $NiCo_2O_4$ nanostructures.

Materials and methods

Materials utilized

All the substances were used exactly as they were obtained, with no further modifications. Potassium hydroxide (KOH) and N-Methyl-2-pyrrolidone (NMP) were purchased with analytical grade from LOBA. Cobalt nitrate hexahydrate ($Co(NO_3)_2.6H_2O$, AVARICE, 98% purity) and nickel nitrate hexahydrate ($Ni(NO_3)_2.6H_2O$, RANKEM, 98% purity) were purchased. The whole experiment was performed with double distilled water.

Synthesis

A simple room temperature co-precipitation synthesis followed by a calcination route was followed to fabricate $NiCo_2O_4$. The illustration for the synthesis is represented in Fig. 1. Initially, 10 mmol of $Ni(NO_3)_2.6H_2O$ and 20 mmol of $Co(NO_3)_2.6H_2O$ were dissolved in 40 ml of double distilled water to prepare solution (I) and stirred magnetically for half-hour. Furthermore, 6 M KOH was prepared in 10 ml for solution (II). After half-hour stirring, solution (II) was dropwise added to the solution (I). The obtained precipitates were left stirred for another 1 h. The precipitates were then filtered and washed multiple times with distilled water and ethanol. The filtrate was dried in an electric oven at 80 °C overnight. Finally, to obtain $NiCo_2O_4$, the dried precipitates were calcined at a temperature of 300 °C for 3 h in a furnace and named NC300. The sample was prepared again to calcined at 500 °C and named NC500.

Electrode preparation

To prepare the electrodes, 80 mg prepared sample, 10 mg activated carbon, and 10 mg polyvinylidene fluoride (PVDF) were taken for each sample and carefully pulverized in a mortar-pestle for 1 h. The mixture was poured into a 10 ml culture tube, which was then sprinkled with 5–6 drops of N-methyl-2-pyrrolidone (NMP). To generate a homogeneous

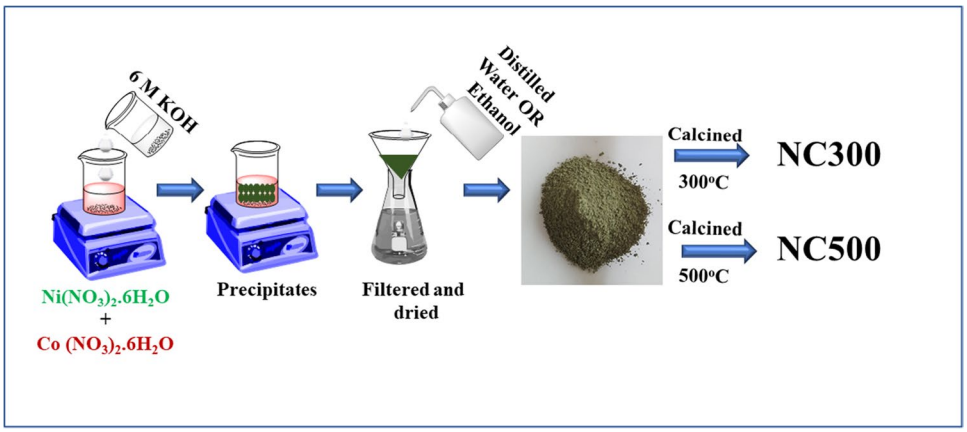

Fig. 1 Schematic diagram for the synthesis of $NiCo_2O_4$ through the Co-precipitation route

slurry, the mixture was magnetically swirled for roughly 12 h. The prepared slurry was dropped onto clean and dry Ni foil in a 1-cm^2 area using the drop-caste method. The pasted electrodes were dried for 12 h in an electric oven at 80 °C. The mass of an empty clean electrode and a slurry pasted, and dried electrodes were used to calculate the weight of active material. The mass of the active material was nearly 1.0 mg.

Characterization techniques

The crystallinity, purity, and structural features of both the manufactured $NiCo_2O_4$ samples were investigated using an X-ray diffractometer (Rigaku Miniflex Japan) with a Cu-K_α radiation source and a scanning rate of 2°/min within the range of 10–90° characterization. For surface, morphological, and elemental composition analyses, the JEOL JSM-6390LV SEM was utilized to achieve scanning electron microscope (SEM) micrographs and energy dispersive X-ray spectroscopy (EDX) spectrum. For the three-electrode (3E) arrangement, the electrochemical investigation was performed using a CHI 760E electrochemical workstation. The synthesized material served as the working electrode, with Ag/AgCl serving as the reference electrode and a platinum wire acting as the counter electrode. Under electrochemical inquiry, cyclic voltammetry (CV), galvanostatic charge–discharge (GCD), and electrostatic impedance spectroscopy (EIS) characterizations are studied in 2 M KOH electrolyte.

Results and discussions

X-ray diffraction (XRD)

XRD characterization was applied to investigate the crystalline nature and purity of the manufactured samples. The obtained XRD patterns for NC300 and NC500 are presented in Fig. 2(a) and the crystal structure of $NiCo_2O_4$ is shown in Fig. 2(b). The diffraction crests in both materials are at 18.7, 31.0, 36.75, 44.50, 55.20, 58.92, 64.7, and 77.8, which

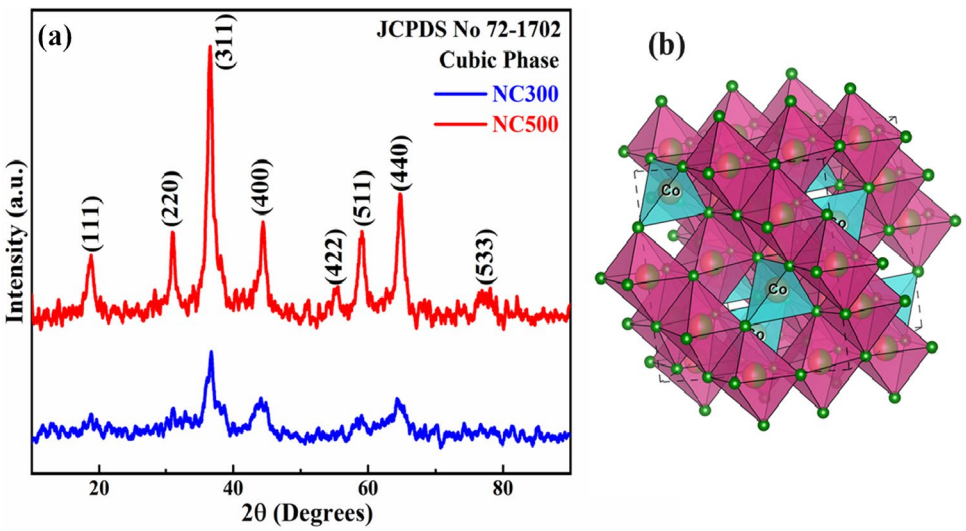

Fig. 2 **a** Room-temperature X-ray diffraction of $NiCo_2O_4$ prepared at 300 °C and 500 °C temperatures. **b** Crystal structure of spinel-like $NiCo_2O_4$

correspond to the (111), (220), (311), (400), (422), (511), (440), and (533) planes, respectively. The result was consistent with the conventional cubic phase $NiCo_2O_4$ pattern (JCPDS number 73–1702) [24]. There were no more peaks seen, indicating the creation of a pure cubic phase. The higher peak intensity in NC500 as compared to NC300 clear indicates the effect of calcination temperature on the crystallinity of the material. A difference in the electrochemical performance can also be predicted from the XRD pattern.

Scanning electron microscope and energy dispersive X-ray analysis (EDAX)

To explore the surface morphology and elemental composition, the synthesized materials have gone through the room temperature SEM and EDAX analysis. The resulted images are revealed in Fig. 3(a–d). The NC300 sample has a non-uniform sheet-like morphology as indicated in Fig. 3(a); on the other hand, comparatively smaller sheets and a few rods are visible in Fig. 3(c) for NC500. The EDAX spectrum of NC300 and NC500 is shown in Fig. 3(b) and Fig. 3(d), respectively, indicating the presence of elements Ni, Co, and O which confirms the purity of the samples. The effect of temperature is noticeable on the morphology as well as the weight percentage of the synthesized samples of $NiCo_2O_4$. Changes in morphology and weight percentage with temperature can produce a significant impact on the electrochemical properties of materials. Sintering at a higher temperature or for longer periods of time can improve crystal development and crystallinity in the sample. As a result, the capacity of calcined materials at higher temperatures is estimated to be greater.

Cyclic voltammetry

CV is a valuable characterization for determining the charge storage mechanism of electrode material. Figure 4(a) and (b) represents the voltammograms of NC300 and NC500, respectively, within a potential window range of 0.0 to 0.45 V (vs. Ag/AgCl electrode) at different scan rates in 1–20 mV/s. Well-defined redox waves belonging to Co^{3+}/Co^{4+} and Ni^{2+}/Ni^{3+} redox couples can be seen in pairs on the CV curves, suggesting battery-type characteristics of the material [25]. At 10 mV/s, the redox couple is positioned at 0.33 V/0.24 V in NC300 and 0.32 V/0.23 V in NC500. The minor discrepancy in redox peak potential is related to differences in morphology. With the increase in scan rates, the shape of voltammograms remains unchanged, while the anodic and cathodic peaks shift towards positive and negative potential, respectively. This shift in peaks is more profound in the case of NC500. A close look at the pattern of NC300 voltammograms shows appropriate redox peaks in both forward and backward sweeps, demonstrating that the electrode material is more reversible and has better rate capability. In the case of NC500, however, the reverse scan peaks are missing, indicating a less reversible nature. The following equations describe the electrochemical behavior of nickel cobaltite ($NiCo_2O_4$) in an alkaline electrolyte [26]:

$$NiCo_2O_4 + OH^- + H_2O \leftrightarrow NiOOH + 2CoOOH + e^- \quad (1)$$

$$NiOOH + OH^- \leftrightarrow NiO_2 + H_2O + e^- \quad (2)$$

$$CoOOH + OH^- \leftrightarrow CoO_2 + H_2O + e^- \quad (3)$$

Co^{3+}/Co^{4+} and M^{2+}/M^{3+} (M = Co and Ni) redox peaks are so close in the potential that they frequently overlap in

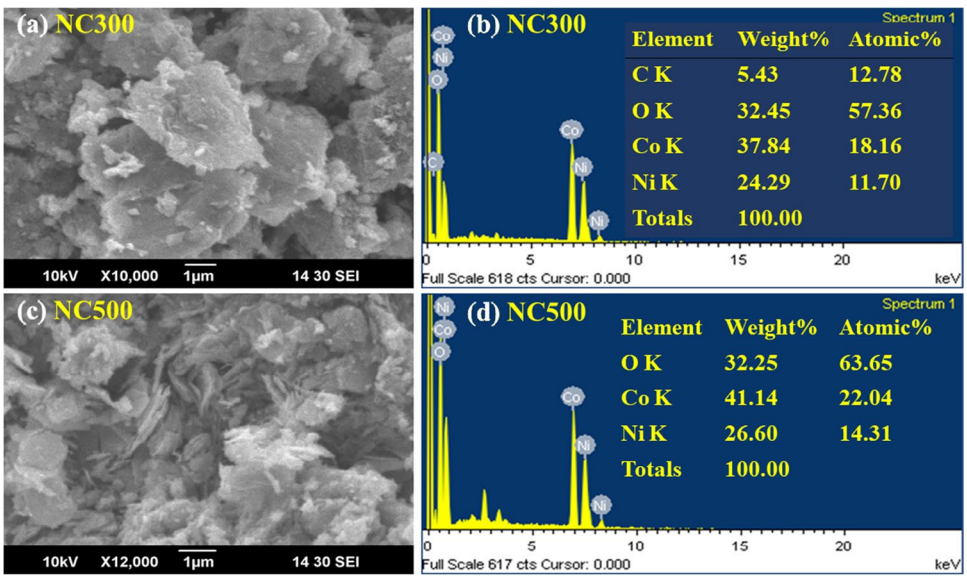

Fig. 3 **a** SEM image of $NiCo_2O_4$ prepared at 300 °C (NC300). **b** EDAX spectrum of NC300. **c** SEM image of $NiCo_2O_4$ prepared at 500 °C (NC500). **d** EDAX spectrum of NC500

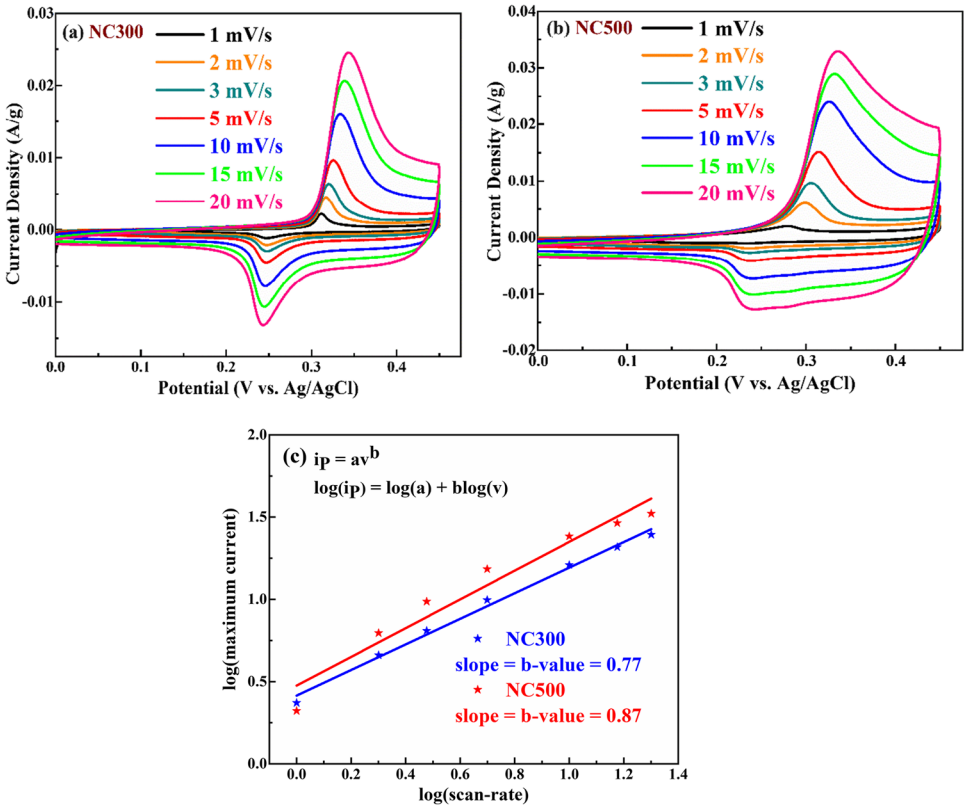

Fig. 4 **a** CV of $NiCo_2O_4$ calcined at 300 °C temperature. **b** CV of $NiCo_2O_4$ calcined at 500 °C temperature. **c** Power-law relationship plot for $NiCo_2O_4$ as NC300 and NC500

the CV pattern and only one peak is observed for all the redox couples.

Furthermore, the power-law relationship, i.e., $i_P = av^b$ (where i_p and v denote the peak current and scan rate, respectively) is investigated to better understand the charge storage mechanism. The "b-value" = 1, nearly 1 (≈ 1), and = 0.5 correspond to pure capacitive EDLC behavior, pseudocapacitive behavior, and battery-like behavior, respectively [27]. Figure 4(c) shows the log(i_P) vs. log(v) plot used to determine the b-value, which is 0.77 for NC300 and 0.87 for NC500, respectively. It can be concluded that the electrochemical behavior of the as-synthesized electrode materials lies mid-way between battery-type and pseudocapacitor. Furthermore, the GCD characterization is used to better assess the reliability of an electrode material in an energy storage application.

Galvanostatic charge–discharge

The charge–discharge behavior, which is evaluated using the Chronopotentiometry technique, is critical for analyzing the practical utility of the material in supercapacitor application. The obtained curves of GCD are represented in Fig. 5(a) and (b) for NC300 and NC500, respectively, within the same potential window as in CV at numerous current densities between 2 and 10 A/g. The quasi-triangular behavior of the curves again confirms the battery-type nature of the electrode materials. Symmetry in charge and discharge arcs indicates the reversibility of the redox reaction. These findings resonate well with the CV observations. The value of specific capacity (C/g) is calculated from the GCD curves using the following equation [28]:

$$C_s = \frac{I}{m} \times \Delta T \tag{4}$$

where C_s is specific capacitance, I/m is current density, and ΔT is the discharge time. Due to the difficulties of reaching all energetic redox sites with a high current density, the discharge time reduces as the current density rises. The calculated values of every specific capacity at several current densities are shown in Table 1. The supreme value of specific capacitance, 224 C/g, is obtained at 2 A/g from NC500, but it is only 100 C/g in NC300. However, NC300 has a rate-performance of 77%, which is higher than 67% in the case of NC500. The variation in the specific capacities with current densities is also elaborated in Fig. 5(c). The cycling stability is another important parameter to judge the practical utility of the electrode material in supercapacitor applications. The NC500 sample results in outstanding retention as shown in Fig. 5(d) of 80% in the specific capacity from the initial after 2000 cycles of GCD at 15.0 A/g current density.

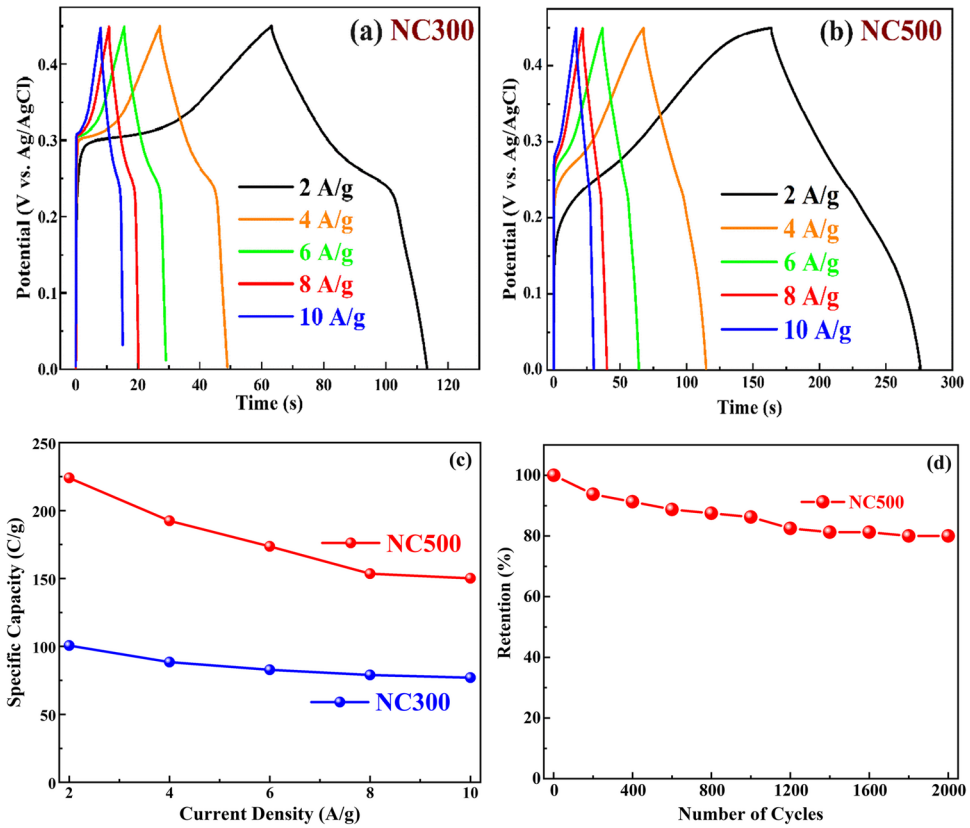

Fig. 5 **a** GCD of $NiCo_2O_4$ calcined at 300 °C temperature. **b** GCD of $NiCo_2O_4$ calcined at 500 °C temperature. **c** Variation in specific capacity (C/g) of $NiCo_2O_4$ with the current density. **d** Retention (%) of $NiCo_2O_4$ as NC500 for 2000 cycles

Table 1 Values of specific capacitance from GCD curves of NC300 and NC500

Sr. no	Current density (A/g)	Specific capacity (C/g)	
		NC300	NC500
1	2	100.6	224.06
2	4	88.52	192.45
3	6	82.80	173.58
4	8	79.04	153.52
5	10	77.00	150.20

Electrostatic impedance spectroscopy

EIS is performed to investigate electrochemical capacitor performance, such as internal resistance, capacity, and so on by applying AC sinusoidal waves. Nyquist plots are used to examine the EIS data which revealed the electrode/electrolyte system's frequency response. The imaginary component (Z") of the impedance is plotted against the real component (Z') in a Nyquist plot. Figure 6(a) shows the EIS data obtained for NC300 and NC500 and the corresponding circuit diagrams are represented in Fig. 6(b) and (c), respectively. A Nyquist plot can be studied in two parts: One is a high-frequency semicircle that represents the charge transfer resistance (R_{CT}) present at the electrode–electrolyte interface, and another is a low-frequency slanted line that arises due to diffusive resistance and capacitive behavior of the material. Hypothetically, a supercapacitor has a straight line at 90° to the real component of the impedance but, practically, it is somewhere between 45 and 90°. For NC300 and NC500, the R_{CT} values determined from the circuit diagram are 43.6 and 21.44 Ω, respectively. The lower capacitance in NC300 is due to a higher R_{CT} value. Furthermore, the equivalent series resistance (R_S) of NC300 is 0.57 Ω which is slightly higher than that of 0.49 Ω for NC500.

Conclusions

In summary, the impact of the temperature of calcination on the electrochemical presentation of spinel-like nickel cobaltite ($NiCo_2O_4$) microstructures was investigated in this study. $NiCo_2O_4$ has been synthesized for this purpose using a robust and simple co-precipitation route at two different temperatures of 300 °C and 500 °C. XRD examination validated the purity of the phase and revealed the increased intensity of diffraction peaks in NC500 that is at the higher temperature of calcination. The electrochemical performance was using a CHI760E electrochemical workstation via CV, GCD, and EIS techniques. In the NC500, the specific capacity was 224 C/g at 2.00 A/g in GCD with 80% retention after 2000

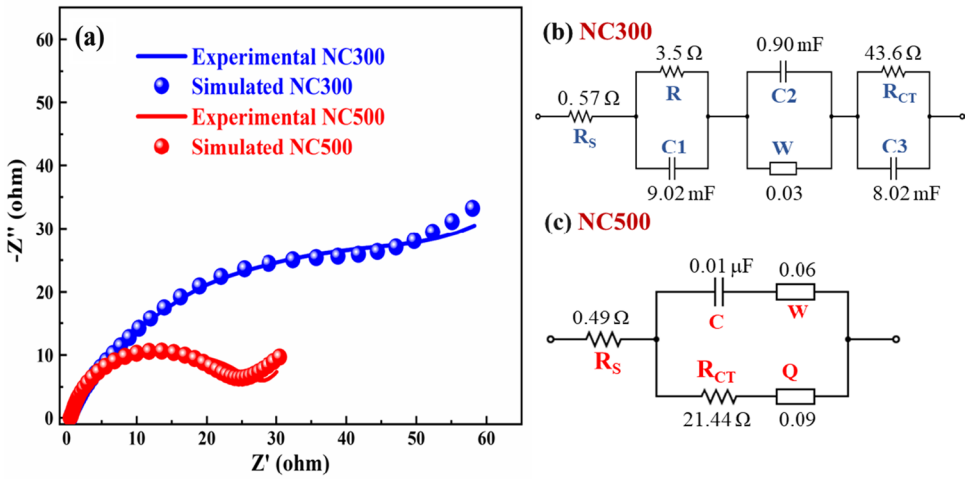

Fig. 6 **a** Nyquist plot $NiCo_2O_4$ calcined at 300 °C (NC300) and 500 °C (NC500) temperature. **b** Equivalent circuit diagram of NC300. **c** Equivalent circuit diagram of NC500

cycles at 15.0 A/g current density. The rate performance of the NC300 was slightly better at 77%, even though the capacitance values in the NC500 were higher. The EIS findings were consistent with the CV and GCD findings. Overall, the electrochemical properties of both samples show that the calcined temperature of 500 °C is suitable for usage as electrode material in supercapacitors.

Acknowledgements One of the authors, P. Chand, is thankful to the Science and Engineering Research Board (SERB), Govt. of India, for providing funding through research project No: SERB/F/10804/2017-18. The authors are also grateful to the Director, NIT Kurukshetra, for providing the facilities in Physics Department. We acknowledge RAFM-2022, organized by the Department of Physics, ARSD College, for this submission.

Author contribution Manpreet Kaur: methodology, software, data curation, and writing – original draft; Prakash Chand: conceptualization, writing – review and editing, validation, resources, and supervision; Hardeep Anand: conceptualization, writing – review and editing, and supervision.

Declarations

Conflict of interest The authors declare no competing interests.

References

1. McCloskey BD, Bethune DS, Shelby RM, Mori T, Scheffler R, Speidel A, Sherwood M, Luntz AC (2012) Limitations in rechargeability of LiO_2 batteries and possible origins. J Phys Chem Lett 3:3043–3047. https://doi.org/10.1021/jz301359t
2. Heubner C, Nikolowski K, Reuber S, Schneider M, Wolter M, Michaelis A (2021) Recent insights into rate performance limitations of Li-ion batteries. Batteries Supercaps 4:268–285. https://doi.org/10.1002/batt.202000227
3. Borenstein A, Hanna O, Attias R, Luski S, Brousse T, Aurbach D (2017) Carbon-based composite materials for supercapacitor electrodes: a review. J Mater Chem A 5:12653–12672. https://doi.org/10.1039/c7ta00863e
4. Sun J, Xu C, Chen H (2021) A review on the synthesis of $CuCo_2O_4$-based electrode materials and their applications in supercapacitors. J Materiomics 7:98–126. https://doi.org/10.1016/j.jmat.2020.07.013
5. Lemine AS, Zagho MM, Altahtamouni TM, Bensalah N (2018) Graphene a promising electrode material for supercapacitors—a review. Int J Energy Res 42:4284–4300. https://doi.org/10.1002/er.4170
6. Yadav S, Devi A (2020) Recent advancements of metal oxides/Nitrogen-doped graphene nanocomposites for supercapacitor electrode materials. J Energy Storage 30:101486. https://doi.org/10.1016/j.est.2020.101486
7. Uke SJ, Akhare VP, Bambole DR, Bodade AB, Chaudhari GN (2017) Recent advancements in the cobalt oxides, manganese oxides, and their composite as an electrode material for supercapacitor: a review. Front Mater 4:2–7. https://doi.org/10.3389/fmats.2017.00021
8. Kouchachvili L, Yaïci W, Entchev E (2018) Hybrid battery/supercapacitor energy storage system for the electric vehicles. J Power Sources 374:237–248. https://doi.org/10.1016/j.jpowsour.2017.11.040
9. Poonam, Sharma K, Arora A, Tripathi SK (2019) Review of supercapacitors: materials and devices. J Energy Storage 21:801–825. https://doi.org/10.1016/j.est.2019.01.010
10. Sun J, Tian X, Xu C, Chen H (2021) Porous $CuCo_2O_4$ microtubes as a promising battery-type electrode material for high-performance hybrid supercapacitors. J Materiomics 7:1358–1368. https://doi.org/10.1016/j.jmat.2021.03.011
11. Chen H, Liu Y, Sun J, Xu C (2021) High-performance hybrid supercapacitor based on the porous copper cobaltite/cupric oxide nanosheets as a battery-type positive electrode material. Int J Hydrogen Energy 46:28144–28155. https://doi.org/10.1016/j.ijhydene.2021.06.056
12. Wu R, Sun J, Xu C, Chen H (2021) $MgCo_2O_4$-based electrode materials for electrochemical energy storage and conversion: a comprehensive review, Sustainable. Energy Fuels 5:4807–4829. https://doi.org/10.1039/d1se00909e
13. Chen H, Du X, Liu X, .Wu R, Li Y, Xu C (2022) Facile growth of nickel foam-supported $MnCo_2O_{4.5}$ porous nanowires as binder-free electrodes for high-performance hybrid supercapacitors. J Energy Storage 50. https://doi.org/10.1016/j.est.2022.104297
14. Kaur M, Chand P, Anand H (2021) Effect of different synthesis methods on morphology and electrochemical behavior of spinel $NiCo_2O_4$ nanostructures as electrode material for energy storage

application. Inorg Chem Commun 134:108996. https://doi.org/10.1016/j.inoche.2021.108996
15. Kumar S, Adinarayana G, Somala R, Sankar S, Mohamed S (2021) Evaluation of pH effect of tin oxide (SnO_2) nanoparticles on photocatalytic degradation, dielectric and supercapacitor applications. J Cluster Sci 7. https://doi.org/10.1007/s10876-021-02092-7
16. Bai Y, Rakhi RB, Chen W, Alshareef HN (2013) Effect of pH-induced chemical modification of hydrothermally reduced graphene oxide on supercapacitor performance. J Power Sources 233:313–319. https://doi.org/10.1016/j.jpowsour.2013.01.122
17. Sunaina, Chand P, Joshi A, Lal S, Singh V (2021) Effect of hydrothermal temperature on structural, optical and electrochemical properties of α-MnO_2 nanostructures for supercapacitor application. Chem Phys Lett 777:138742. https://doi.org/10.1016/j.cplett.2021.138742
18. Qin H, Liu P, Chen C, Cong HP, Yu SH (2021) A multi-responsive healable supercapacitor. Nat Commun 12. https://doi.org/10.1038/s41467-021-24568-w
19. Xu K, Yang J, Hu J (2018) Synthesis of hollow $NiCo_2O_4$ nanospheres with large specific surface area for asymmetric supercapacitors. J Colloid Interface Sci 511:456–462. https://doi.org/10.1016/j.jcis.2017.09.113
20. Wang Z, Su H, Liu F, Chu X, Yan C, Gu B, Huang H, Yang T, Chen N, Han Y, Deng W, Zhang H, Yang W (2019) Establishing highly-efficient surface faradaic reaction in flower-like $NiCo_2O_4$ nano-/micro-structures for next-generation supercapacitors. Electrochim Acta 307:302–309. https://doi.org/10.1016/j.electacta.2019.03.227
21. Zhao N, Fan H, Ma J, Zhang M, Wang C, Li H, Jiang X, Cao X (2019) Entire synergistic contribution of electrodeposited battery-type $NiCo_2O_4$@$Ni_{4.5}Co_{4.5}S_8$ composite for high-performance supercapacitors. J Power Sources 439. https://doi.org/10.1016/j.jpowsour.2019.227097
22. Chen H, Jiang J, Zhang L, Qi T, Xia D, Wan H (2014) Facilely synthesized porous $NiCo_2O_4$ flowerlike nanostructure for high-rate supercapacitors. J Power Sources 248:28–36. https://doi.org/10.1016/j.jpowsour.2013.09.053
23. Manalu A (2022) Synthesis, Microstructure and electrical properties of $NiCo_2O_4$/rGO composites as pseudocapacitive electrode for supercapacitors. Int J Electrochem Sci:22036. https://doi.org/10.20964/2022.03.11
24. Kaur M, Chand P, Anand H (2021) Facile synthesis of $NiCo_2O_4$ nanostructure with enhanced electrochemical performance for supercapacitor application. Chem Phys Lett 786:139181. https://doi.org/10.1016/j.cplett.2021.139181
25. Gupta RK, Candler J, Palchoudhury S, Ramasamy K, Gupta BK (2015) Flexible and high performance supercapacitors based on $NiCo_2O_4$ for wide temperature range applications. Sci Rep 5:1–11. https://doi.org/10.1038/srep15265
26. Wang X, Fang Y, Shi B, Huang F, Rong F, Que R (2018) Three-dimensional $NiCo_2O_4$@$NiCo_2O_4$ core–shell nanocones arrays for high-performance supercapacitors. Chem Eng J 344:311–319. https://doi.org/10.1016/j.cej.2018.03.061
27. Xie J, Yang P, Wang Y, Qi T, Lei Y, Li CM (2018) Puzzles and confusions in supercapacitor and battery: theory and solutions. J Power Sources 401:213–223. https://doi.org/10.1016/j.jpowsour.2018.08.090
28. Yuan C, Li J, Hou L, Zhang X, Shen L, Lou XW (2012) Ultrathin mesoporous $NiCo_2O_4$ nanosheets supported on Ni foam as advanced electrodes for supercapacitors. Adv Funct Mater 22:4592–4597. https://doi.org/10.1002/adfm.201200994